

Banner appropriate to article type will appear here in typeset article

# Helmholtz decompositions of horizontal structure functions including components associated with cyclone-anticyclone symmetry breaking

Erik Lindborg<sup>†</sup>

Department of Engineering Mechanics, KTH, Osquars backe 18, SE-100 44, Stockholm, Sweden

(Received xx; revised xx; accepted xx)

In recent years, several studies have been made in which atmospheric and oceanic data were used to decompose horizontal velocity statistics into a rotational component, associated with vertical vorticity, and a divergent component, associated with horizontal divergence. Making the assumption of statistical homogeneity in a horizontal plane, this can be accomplished by relating the rotational and divergent components of the difference between the velocities at two points to the corresponding longitudinal and transverse components, where the longitudinal and transverse directions are parallel respectively perpendicular to the line between the points. In previous studies, the decomposition has most often been made under the assumption of statistical isotropy. Some attempts have also been made to analyse the anisotropic problem. We derive the full anisotropic equations relating the rotational, divergent and the rotational-divergent components of the second order structure functions to the longitudinal, transverse and longitudinal-transverse components and solve the equations analytically. We also derive some results for third order structure functions, with special focus on the components associated with cyclone-anticyclone asymmetry. Based on the analysis of these components and results from previous analyses of aircraft data, it is concluded that there is an exclusively rotational flow component that is giving rise to strong dominance of cyclonic motions in the upper troposphere and a strong dominance of anticyclonic motions in the lower stratosphere in the range of scales from ten to one thousand km.

## 1. Introduction

A common view of geophysical flows is that they can restlessly be decomposed into a quasigeostrophic component associated with slow ‘balanced’ motions and a component consisting of inertia-gravity waves, whose dynamics evolves over faster time scales. This view has been challenged by the author of the present paper, who has argued that the mesoscale ( $\sim 1 - 500$  km) dynamics in the upper troposphere and lower stratosphere is built up of motions that do not fit into any of these two categories (Lindborg 2006). A useful method to analyse the issue is to decompose observational horizontal velocity statistics into a rotational component, associated with vertical vorticity, and a divergent component, associated with horizontal divergence. Quasigeostrophic motions are exclusively rotational while linear gravity waves are exclusively divergent. Inertia-gravity waves have a rotational

<sup>†</sup> Email address for correspondence: erikl@mech.kth.se

component. However, this is weak for waves with frequencies that are not very close to the inertial frequency.

The statistics of two-point velocity measurements are commonly divided into a longitudinal component, which is parallel to the line between the points, and a transverse component, which is perpendicular. The idea that the ratio between vortical and divergent energy can be estimated by measuring the ratio,  $E_{ll}/E_{tt}$ , between the longitudinal and transverse velocity wave number spectra was formulated by Eckermann (1990) who argued that a ratio smaller than unity is an indication of dominance of vortical energy. The idea was further developed by Cho and Newell (1999) who calculated  $E_{ll}/E_{tt}$  in the mesoscale range using aircraft data from the Pacific Ocean at altitudes between 2 and 12 km. An average over these altitudes gave  $E_{ll}/E_{tt} \approx 0.8$ . Based on this observation, they argued that vortical energy is dominant. A more systematic Helmholtz decomposition method was introduced by Lindborg (2007), who, under the assumption of isotropy, derived the equations relating two-point covariances of vorticity and horizontal divergence to the longitudinal and transverse second order structure functions. The longitudinal structure function is the second order statistical moment of the difference between the longitudinal velocity component at two points and the transverse structure function is the corresponding moment for the component in a perpendicular direction. Using structure function data from the upper troposphere and lower stratosphere calculated by Lindborg (1999) it was possible to estimate the two-point covariances of vorticity and divergence as well as the corresponding spectra. Lindborg (2007) concluded that the  $k^{-5/3}$  mesoscale energy spectra in the upper troposphere and lower stratosphere, that was measured by Nastrom and Gage (1985), cannot be generated by a field of inertia-gravity waves, since the rotational component is of the same order of magnitude as the divergent component. A method similar to the one developed by Lindborg (2007), but completely expressed in Fourier space, was developed by Bühler et al. (2014) who used it to analyse ship data from the ocean. The method was also used by Callies et al. (2014) to analyse aircraft data from the upper troposphere and lower stratosphere. Callies et al. (2014) obtained results that were consistent with the results of Lindborg (2007), with a rotational component that was of the same order of magnitude as the divergent component in the mesoscale range. However, they interpreted the results differently, and made the hypothesis that the spectra are generated by inertia-gravity waves with frequencies very close to the inertial frequency. Lindborg (2015) showed that the two methods are equivalent and derived simplified closed expressions relating the rotational and divergent structure functions, two-point covariances as well as spectra to the corresponding longitudinal and transverse quantities that can be directly evaluated from observational data. The Helmholtz decomposition method has subsequently been used, either in structure function formulation or spectral formulation, to analyse oceanic ship data (Bühler et al. 2017; Vladoiu et al. 2024), data from Lagrangian drifters in the ocean (Pearson et al. 2019; Wang and Bühler 2021), data from a mooring array in the ocean (Callies et al. 2020), aircraft data from the upper troposphere and lower stratosphere (Callies et al. 2016; Li and Lindborg 2018), and radar data from the mesosphere and lower troposphere (Poblet et al. 2023).

Some attempts have also been made to analyse the anisotropic problem. Bühler et al. (2017) used a model to derive formulas by which the one-dimensional spectral decomposition relations were corrected by a term including effects of anisotropy and used the model in the analysis of ship data. It is, however, unclear to the author if it is possible to include such corrections based on one-dimensional data. Wang and Bühler (2021) developed a method by which inversion formulas for the anisotropic rotational and divergent second order structure functions were guessed at under the assumption that vorticity and divergence either are uncorrelated or isotropically correlated. They verified the formulas by the aid of computer algebra and used them in the analysis of data from Lagrangian drifters in the ocean.

Isotropy is commonly defined as invariance with respect to rotations and reflections. In this context, this should be interpreted as invariance under rotations with respect to vertical axes and reflections in vertical planes, while in the context of three-dimensional problems it should be interpreted as invariance under rotations with respect to any axis and reflections in any plane. In three-dimensional turbulence theory, interesting insights can be gained by dropping the constraint of reflectional invariance. The statistical analysis of helicity, which is the scalar product of velocity and vorticity, is commonly made under the assumption of rotational but not reflectional invariance, since helicity changes sign under reflections. In a similar way, dropping the constraint of reflectional invariance for horizontal velocity statistics allows us to study the interesting problem of cyclone-anticyclone symmetry breaking in geophysical flows.

The aim of the present paper is twofold. First, we will formulate the complete anisotropic decomposition problem for second order structure functions including the component that is antisymmetric with respect to reflections, and solve the problem. Second, assuming rotational but not reflectional invariance, we will analyse the problem of finding a scale dependent measure of the degree to which cyclone-anticyclone symmetry is broken in a geophysical flow and show that second order statistics alone cannot provide such a measure, but third order statistics is required.

## 2. Helmholtz decompositions

### 2.1. Second order structure functions

We define the horizontal velocity increment between two points separated by a vector  $\mathbf{r}$  in a horizontal plane as

$$\delta\mathbf{u} = \mathbf{u}(\mathbf{x} + \mathbf{r}) - \mathbf{u}(\mathbf{x}), \quad (2.1)$$

and consider an ensemble of velocity increments for which  $\mathbf{r}$  is oriented at an angle  $\theta$  relative to some fixed horizontal axis. Each increment in the ensemble can then be expressed as  $\delta\mathbf{u} = \mathbf{e}_l\delta u_l + \mathbf{e}_t\delta u_t$ , where  $\mathbf{e}_l = \mathbf{r}/r$  is the radial or ‘longitudinal’ unit vector and  $\mathbf{e}_t$  is the azimuthal or ‘transverse’ unit vector, defined as  $\mathbf{e}_t = \mathbf{e}_z \times \mathbf{e}_l$  (where  $\mathbf{e}_z$  is the vertical unit vector). If the right hand rule is used to calculate the cross product,  $\delta u_t$  will be positive/negative for cyclonic/anticyclonic motions on the northern hemisphere and vice versa on the southern hemisphere, just as vertical vorticity. It may be a good idea to use a left hand rule for the cross product on the southern hemisphere, so that  $\delta u_t$  as well as vertical vorticity always is positive for cyclonic motions. Cho and Lindborg (2001) used the opposite convention, defining  $\delta u_t$  so that it is negative for cyclonic motions. The second order horizontal structure function tensor is defined as  $\mathbf{D} = \langle \delta\mathbf{u}\delta\mathbf{u} \rangle$ , where  $\langle \rangle$  denotes the ensemble average. Assuming statistical homogeneity in a horizontal plane,  $\mathbf{D}$  is independent of  $\mathbf{x}$  and is even in  $\mathbf{r}$ , that is  $\mathbf{D}(-\mathbf{r}) = \mathbf{D}(\mathbf{r})$ . The structure function tensor can be expressed as

$$\mathbf{D}(\mathbf{r}) = \mathbf{e}_l\mathbf{e}_l D_{ll}(r, \theta) + \mathbf{e}_t\mathbf{e}_t D_{tt}(r, \theta) + (\mathbf{e}_l\mathbf{e}_t + \mathbf{e}_t\mathbf{e}_l) D_{lt}(r, \theta), \quad (2.2)$$

where  $D_{ll} = \langle \delta u_l \delta u_l \rangle$  and  $D_{tt} = \langle \delta u_t \delta u_t \rangle$  are reflectionally symmetric and  $D_{lt} = \langle \delta u_l \delta u_t \rangle$  is reflectionally antisymmetric.

$\mathbf{D}$  can be expressed in an alternative way, by making a Helmholtz decomposition of the horizontal velocity field,

$$\mathbf{u} = \mathbf{u}_r + \mathbf{u}_d, \quad (2.3)$$

where

$$\mathbf{u}_r = -\mathbf{e}_z \times \nabla\psi, \quad \mathbf{u}_d = \nabla\phi. \quad (2.4)$$

Here,  $\psi$  is the stream function,  $\phi$  is the velocity potential, and  $\nabla$  is the two-dimensional gradient operator. We can now express the structure function tensor as

$$\mathbf{D}(\mathbf{r}) = \langle \delta \mathbf{u}_r \delta \mathbf{u}_r \rangle + \langle \delta \mathbf{u}_d \delta \mathbf{u}_d \rangle + \langle \delta \mathbf{u}_r \delta \mathbf{u}_d \rangle + \langle \delta \mathbf{u}_d \delta \mathbf{u}_r \rangle. \quad (2.5)$$

In this representation,  $\mathbf{D}$  is determined by three scalar functions

$$D_{rr} = \langle \delta \mathbf{u}_r \cdot \delta \mathbf{u}_r \rangle, \quad D_{dd} = \langle \delta \mathbf{u}_d \cdot \delta \mathbf{u}_d \rangle, \quad D_{dr} = \mathbf{e}_z \cdot \langle \delta \mathbf{u}_d \times \delta \mathbf{u}_r \rangle. \quad (2.6)$$

In Appendix A show that these functions are related to the two-point covariances of vertical vorticity,  $\zeta = -\nabla^2 \psi$ , and horizontal divergence,  $d = \nabla^2 \phi$ , as

$$\nabla^2 D_{rr} = 2 \langle \zeta \zeta' \rangle, \quad (2.7)$$

$$\nabla^2 D_{dd} = 2 \langle dd' \rangle, \quad (2.8)$$

$$\nabla^2 D_{dr} = \langle \zeta d' + \zeta' d \rangle, \quad (2.9)$$

where primed quantities are evaluated at a distance  $r$  from unprimed quantities. The Laplace operator in (2.7-2.9) is operating on the coordinates of the separation vector. For example,

$$\nabla^2 D_{rr} = \frac{1}{r} \frac{\partial}{\partial r} \left( r \frac{\partial D_{rr}}{\partial r} \right) + \frac{1}{r^2} \frac{\partial^2 D_{rr}}{\partial \theta^2}. \quad (2.10)$$

It is straightforward to show that  $\langle \delta \mathbf{u}_r \cdot \delta \mathbf{u}_d \rangle = 0$ , by homogeneity. We therefore have

$$D_{rr} + D_{dd} = D_{ll} + D_{tt}. \quad (2.11)$$

The equations relating  $D_{rr}$ ,  $D_{dd}$  and  $D_{dr}$  on the one hand to  $D_{ll}$ ,  $D_{tt}$  and  $D_{lt}$  on the other hand are derived in Appendix A using the method developed by Lindborg (2007). They can be formulated as

$$\nabla^2 D_{rr} = \nabla^2 D_{ll} + \frac{1}{r^2} \frac{\partial}{\partial r} \left( r^2 \frac{\partial (D_{tt} - D_{ll})}{\partial r} \right) - \frac{2}{r^2} \frac{\partial}{\partial r} \left( r \frac{\partial D_{lt}}{\partial \theta} \right), \quad (2.12)$$

$$\nabla^2 D_{dd} = \nabla^2 D_{tt} - \frac{1}{r^2} \frac{\partial}{\partial r} \left( r^2 \frac{\partial (D_{tt} - D_{ll})}{\partial r} \right) + \frac{2}{r^2} \frac{\partial}{\partial r} \left( r \frac{\partial D_{lt}}{\partial \theta} \right), \quad (2.13)$$

$$\nabla^2 D_{dr} = \frac{1}{r^2} \frac{\partial}{\partial r} \left( r^2 \frac{\partial D_{lt}}{\partial r} \right) + \frac{1}{r} \frac{\partial D_{lt}}{\partial r} - \frac{1}{r^2} \frac{\partial^2 D_{lt}}{\partial \theta^2} + \frac{1}{r^2} \frac{\partial^2}{\partial r \partial \theta} (r (D_{tt} - D_{ll})). \quad (2.14)$$

The equations can be solved as Fourier series. To do this, we introduce a function  $f(r, \theta)$  to represent any of the functions  $D_{rr}$ ,  $D_{dd}$ ,  $D_{rd}$ ,  $D_{tt}$ ,  $D_{ll}$  or  $D_{lt}$ . Since  $\mathbf{D}$  is even in  $\mathbf{r}$ , we must have  $f(r, \theta) = f(r, \theta + \pi)$ . Expanding  $f$  in a Fourier series over the interval  $\theta \in [0, 2\pi]$ , odd modes must therefore be zero. Thus, we can make the expansion

$$f(r, \theta) = \sum_{n=2k} f^{cn}(r) \cos(n\theta) + f^{sn}(r) \sin(n\theta), \quad (2.15)$$

where  $k = 0, 1, 2, 3 \dots$ , and

$$f^{c0}(r) = \frac{1}{2\pi} \int_0^{2\pi} f(r, \theta) d\theta, \quad (2.16)$$

$$f^{cn}(r) = \frac{1}{\pi} \int_0^{2\pi} f(r, \theta) \cos(n\theta) d\theta \quad n \neq 0, \quad (2.17)$$

$$f^{sn}(r) = \frac{1}{\pi} \int_0^{2\pi} f(r, \theta) \sin(n\theta) d\theta \quad n \neq 0. \quad (2.18)$$

The solutions for the zero modes are,

$$D_{rr}^{c0}(r) = D_{tt}^{c0}(r) + \int_0^r \tau^{-1} \left( D_{tt}^{c0}(\tau) - D_{ll}^{c0}(\tau) \right) d\tau, \quad (2.19)$$

$$D_{dd}^{c0}(r) = D_{ll}^{c0}(r) - \int_0^r \tau^{-1} \left( D_{tt}^{c0}(\tau) - D_{ll}^{c0}(\tau) \right) d\tau, \quad (2.20)$$

$$D_{dr}^{c0}(r) = D_{lt}^{c0}(r) + 2 \int_0^r \tau^{-1} D_{lt}^{c0}(\tau) d\tau. \quad (2.21)$$

The solutions (2.19-2.20) are identical to the isotropic solutions derived by Lindborg (2015). The expressions (2.19-2.21) are the solutions to the angular averaged equations. From a practical point of view, they can thus be used in the analysis of highly anisotropic flows, provided that the structure functions are carefully averaged over all angles.

In the limit  $r \rightarrow 0$ , the Fourier modes of  $D_{tt}$ ,  $D_{ll}$  and  $D_{lt}$  go to zero as  $\sim r^2$ . It is obvious that (2.19-2.21) have the same property. To show that the integrals converge in the limit  $r \rightarrow \infty$  we write  $u_l = u \cos \theta + v \sin \theta$ ,  $u_t = -\sin \theta u + \cos \theta v$ , where  $u$  and  $v$  are the Cartesian velocity components, and note that

$$D_{ll} = -2\langle u_l u_l' \rangle + \langle u^2 \rangle + \langle v^2 \rangle + \cos(2\theta) \left( \langle u^2 \rangle - \langle v^2 \rangle \right) + 2 \sin(2\theta) \langle uv \rangle, \quad (2.22)$$

$$D_{tt} = -2\langle u_t u_t' \rangle + \langle u^2 \rangle + \langle v^2 \rangle - \cos(2\theta) \left( \langle u^2 \rangle - \langle v^2 \rangle \right) - 2 \sin(2\theta) \langle uv \rangle, \quad (2.23)$$

$$D_{lt} = -\langle u_l u_t' \rangle - \langle u_t u_l' \rangle + 2 \cos(2\theta) \langle uv \rangle + \sin(2\theta) \left( \langle v^2 \rangle - \langle u^2 \rangle \right). \quad (2.24)$$

In the limit of large  $r$ , the integrands will therefore go to zero as  $2\tau^{-1}(\langle u_t u_t' \rangle - \langle u_l u_l' \rangle)$  and  $-\tau^{-1}(\langle u_l u_t' \rangle + \langle u_t u_l' \rangle)$ , and the integrals will therefore converge. To accurately calculate the integrals in (2.19-2.21) we would need full knowledge of the structure functions in the interval  $\tau \in [0, r]$ . In reality, we have to set the lower integration limit to the smallest separation,  $r_{min}$ , for which the structure functions can be calculated, which is determined by the resolution of the data. It can be argued that the error caused by such a replacement will be quite small (Lindborg 2015).

The solutions for the non-zero modes are derived in Appendix B. They are quite intricate and involve terms of the types

$$(p-1)r^{-p} \int_0^r \tau^{p-1} f^p(\tau) d\tau, \quad (p+1)r^p \int_r^\infty \tau^{-p-1} f^p(\tau) d\tau, \quad (2.25)$$

where  $f^p$  is a Fourier mode of  $D_{ll}$ ,  $D_{tt}$  or  $D_{lt}$ . For the first type of term, the error will be even smaller than the corresponding errors for the zero mode, when the lower integration limit is replaced by  $r_{min}$ . To calculate the second type of integrals we have to replace the upper integration by the largest separation,  $r_{max}$ , for which statistical homogeneity can be assumed to hold. In the upper troposphere and lower stratosphere, a reasonable estimate is  $r_{max} \approx 2000$  km. Wang and Bühler (2021) derived solutions for the non-zero modes under the assumption that vorticity and divergence are either uncorrelated or isotropically correlated, which can be formulated as  $\partial_\theta \nabla^2 D_{dr} = 0$ . They used a completely different method than the one we have used. Instead of deriving (2.12) and (2.13), Wang and Bühler (2021) used Cartesian coordinates to relate two-point covariances of Cartesian velocity components to derivatives of two-point covariances involving  $\phi$  and  $\psi$ . The expressions were transformed to polar coordinates and inversion formulas for the Fourier modes of  $D_{rr}$  and  $D_{ll}$  were then guessed at and verified by computer algebra. The solutions do not involve any integrals of the types (2.25), only integrals of the same type as in the zero-mode solutions. In Appendix

**C** we confirm that the solutions derived by Wang and Bühler (2021) are correct, under the assumption which they were derived.

The spectral counterpart of the solution (2.24) for the reflectionally antisymmetric component is

$$E_{dr}(k) = E_{lt}(k) + \frac{2}{k} \int_k^\infty E_{lt}(\tilde{k}) d\tilde{k}, \quad (2.26)$$

where  $E_{dr}$  is the one-dimensional divergent-rotational cospectrum and  $E_{lt}$  is the one-dimensional longitudinal-transverse cospectrum that can be directly calculated from aircraft or ship data. Calculations of either  $D_{dr}(r)$  or  $E_{dr}(k)$  from observational data may or may not provide new interesting insights into the dynamics of geophysical flows and the way cyclone-anticyclone symmetry is broken. Wang and Bühler (2021) calculated  $D_{lt}$  using data from Lagrangian drifters in the ocean and suggested that it can provide us with insights into the degree of ‘spirality’ of the flow, which has been studied by Zhurbas et al. (2019). On the other hand, Cho and Lindborg (2001) and Lindborg and Cho (2001) calculated  $D_{lt}$  from aircraft data and found that the ratio  $|D_{lt}|/D_{tt}$  was less than 2% for  $r < 100$  km and less than 5% for  $r < 2000$  km. A plot of  $D_{lt}$  from these analyses communicated by J. Cho to the author showed no consistent sign or functional dependence in different latitude bands in the upper troposphere and lower stratosphere. It is quite clear that  $D_{lt}$  can give us only limited information on cyclone-anticyclone asymmetry, since it only tells us to what degree divergence and vorticity are correlated. It may very well be that  $D_{lt}$  is zero in a flow with strong preference for either cyclonic or anticyclonic motions. To define a scale dependent measure of the degree to which cyclone-anticyclone symmetry is broken we need a measure that is not zero in case divergence is zero or uncorrelated with vorticity. To define such a measure we need third order structure functions.

## 2.2. Third order structure functions

We define the third order structure function tensor as  $\mathbf{D}^{(3)} = \langle \delta \mathbf{u} \delta \mathbf{u} \delta \mathbf{u} \rangle$  and resolve it as

$$\begin{aligned} \mathbf{D}^{(3)}(\mathbf{r}) = & \mathbf{e}_l \mathbf{e}_l \mathbf{e}_l D_{lll}(r, \theta) + (\mathbf{e}_l \mathbf{e}_t \mathbf{e}_t + \mathbf{e}_t \mathbf{e}_l \mathbf{e}_t + \mathbf{e}_t \mathbf{e}_t \mathbf{e}_l) D_{ltt}(r, \theta) \\ & + \mathbf{e}_t \mathbf{e}_t \mathbf{e}_t D_{ttt}(r, \theta) + (\mathbf{e}_t \mathbf{e}_l \mathbf{e}_l + \mathbf{e}_l \mathbf{e}_t \mathbf{e}_l + \mathbf{e}_l \mathbf{e}_l \mathbf{e}_t) D_{tll}(r, \theta), \end{aligned} \quad (2.27)$$

where  $D_{lll} = \langle (\delta u_l)^3 \rangle$  and  $D_{ltt} = \langle \delta u_l (\delta u_t)^2 \rangle$  are reflectionally symmetric while  $D_{ttt} = \langle (\delta u_t)^3 \rangle$  and  $D_{tll} = \langle \delta u_t (\delta u_l)^2 \rangle$  are reflectionally antisymmetric. By homogeneity,  $\mathbf{D}^{(3)}$  is independent of  $\mathbf{x}$  and odd in  $\mathbf{r}$ , that is  $\mathbf{D}^{(3)}(-\mathbf{r}) = -\mathbf{D}^{(3)}(\mathbf{r})$ , implying that each of  $D_{lll}$ ,  $D_{ltt}$ ,  $D_{ttt}$  and  $D_{tll}$  has the same value at  $\theta + \pi$  and  $\theta$ . We will not make any complete Helmholtz decomposition of the components of  $\mathbf{D}^{(3)}$ , but only derive some relations that may be useful in future investigations, assuming rotational but not reflectional invariance. In particular, we will focus on the components  $D_{ttt}$  and  $D_{tll}$  that are associated with cyclone-anticyclone asymmetry. We start by forming two second order tensors,  $\mathbf{P}$  and  $\mathbf{Q}$ , by projecting  $\mathbf{D}^{(3)}$  onto the the horizontal divergence and the vertical vorticity operators. We give the definitions in Cartesian tensor notation

$$P_{ij} = \nabla_k D_{kij}^{(3)}, \quad (2.28)$$

$$Q_{ij} = \epsilon_{3km} \nabla_k D_{mij}^{(3)}. \quad (2.29)$$

Assuming that  $D_{lll}$ ,  $D_{ltt}$ ,  $D_{ttt}$  and  $D_{tll}$  have no dependence on  $\theta$  (rotational invariance) it is straightforward to express the components of  $\mathbf{P}$  and  $\mathbf{Q}$  in terms of the components of  $\mathbf{D}^{(3)}$ . A calculation is carried out in Appendix D. In principle, we could use the analysis in the previous section to make full Helmholtz decompositions of  $\mathbf{P}$  and  $\mathbf{Q}$ . However, we will

refrain from doing this, but only use the analysis in the previous section to derive relations that hold for an exclusively rotational field and an exclusively divergent field.

In total, there are four independent Helmholtz decomposed components of  $\mathbf{P}$  and  $\mathbf{Q}$ . These are  $P_{dd}, P_{rr}, P_{dr}$  and  $Q_{rr}$ . It is straightforward to show that  $Q_{dd} = P_{dr}$  and  $Q_{dr} = P_{rr}$  (see Appendix D). For a rotational field we must have

$$P_{dd} = P_{dr} = 0. \quad (2.30)$$

These conditions give us the relations (see Appendix D),

$$D_{ltt} = \frac{r}{3} \frac{dD_{lll}}{dr}, \quad (2.31)$$

$$D_{ttt} = \frac{1}{r} \frac{d}{dr} \left( r^2 D_{tll} \right), \quad (2.32)$$

for an exclusively rotational field. The relation (2.31) was previously derived by Lindborg (1999), using a slightly different method. We note that there is a single independent component, either  $D_{ttt}$  or  $D_{tll}$ , that is associated with cyclone-anticyclone asymmetry. For a divergent field we must have

$$P_{rr} = P_{dr} = Q_{rr} = 0. \quad (2.33)$$

These conditions give us the relations (see Appendix D),

$$D_{lll} = \frac{1}{r} \frac{d}{dr} \left( r^2 D_{ltt} \right), \quad (2.34)$$

$$D_{ttt} = D_{tll} = 0, \quad (2.35)$$

for an exclusively divergent field. We note that there is no component that is associated with cyclone-anticyclone asymmetry.

Cho and Lindborg (2001) and Lindborg and Cho (2001) calculated all four components of  $\mathbf{D}^{(3)}$  in the upper troposphere and lower stratosphere. For the reflectionally symmetric components,  $D_{lll}$  and  $D_{ltt}$ , the results were not very well converged, due to strong cancellations, especially in the upper troposphere. In the lower stratosphere, Cho and Lindborg (2001) were able to obtain reasonably well converged results for the sum  $D_{lll}(r) + D_{ltt}(r)$  in the range  $r \in [10, 200]$  km, showing a negative sign and a linear dependence on  $r$ . This result was interpreted as evidence of a downscale energy cascade. Similar results were subsequently obtained in numerical simulations of rotating stratified turbulence at Rossby number of the order of unity, exhibiting a downscale energy cascade (Deusebio et al. 2014), supporting such an interpretation.

Quite surprisingly, the results for the reflectionally antisymmetric components,  $D_{ttt}$  and  $D_{tll}$ , showed much better convergence, with a strong preference for cyclonic motions in the upper troposphere and strong preference for anticyclonic motions in the lower stratosphere. Both  $D_{ttt}$  and  $D_{tll}$  showed an approximate  $r^2$ -dependence in the range  $r \in [10, 1000]$  km, but with different signs in the two regions. These results were reproduced (but not published) in the data analysis carried out by Li and Lindborg (2018). As a matter of fact, Lindborg and Cho (2001) also used the results to calculate the right hand side of (2.32) numerically and found a very good agreement with the left hand side, both in the upper troposphere and the lower stratosphere (see fig. 1 and fig. 2 in Lindborg and Cho 2001). The reason why this calculation was carried out was that the quantity

$$D_{ttt} - \frac{1}{r} \frac{d}{dr} \left( r^2 D_{tll} \right), \quad (2.36)$$

appeared in the dynamical equation for  $D_{lt}$  that was derived by Lindborg and Cho (2001).

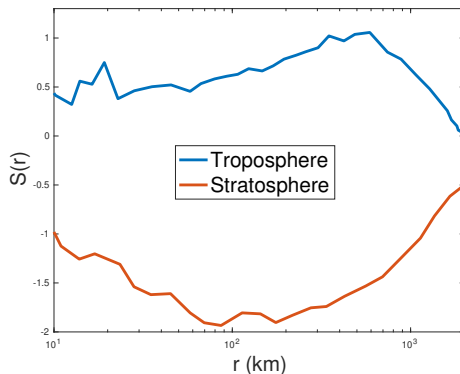


Figure 1: Skewness of the transverse velocity component as a function of  $r$  calculated from all transverse structure functions evaluated by Cho and Lindborg (2001).

The observation that there is an almost perfect cancellation between the two terms in (2.36) was presented as an unexplained mystery by Lindborg and Cho (2001). In the light of the present analysis, the interpretation is clear. Cyclone-anticyclone symmetry is broken exclusively by rotational or vortical motions. The reason why the quantity (2.36) appears in the dynamical equation for  $D_{lt}$  is that  $D_{lt}$  is exclusively coupled to  $D_{rd}$  which is zero for a rotational field. There is zero or weak nonlinear generation of  $D_{dr}$ .

A commonly used measure of the degree of cyclone-anticyclone asymmetry is the skewness of vertical vorticity,  $S_\zeta = \langle \zeta^3 \rangle / \langle \zeta^2 \rangle^{3/2}$ . This measure has obvious drawbacks. In case the energy spectra are more shallow than  $\sim k^{-3}$  (or the structure functions are more shallow than  $\sim r^2$ ), as in atmospheric mesoscale flows, vorticity is totally dominated by the smallest scales under consideration. If we increase the resolution in a data analysis or a numerical simulation, we will find that the magnitude of the estimated vorticity increases. In a fully resolved data analysis or numerical simulation vorticity would peak at the Kolmogorov scale, which can be estimated to a few millimetres. Clearly, we need another measure, putting more weight on larger scales and also carrying information on the degree of symmetry breaking as a function of scale. Such a measure is provided by the skewness of the transverse velocity component,

$$S(r) = \frac{\langle \delta u_t^3 \rangle}{\langle \delta u_t^2 \rangle^{3/2}}. \quad (2.37)$$

In figure 1, we have plotted  $S(r)$  in the range  $r \in [10, 2000]$  km, calculated from all transverse structure functions evaluated by Cho and Lindborg (2001). In the upper troposphere, data were collected at all latitudes, with a dominance of mid-latitudes on the northern hemisphere while in the lower stratosphere data were collected at latitudes larger than thirty degrees (northern and southern hemisphere). The sign convention used in the figure is that positive values corresponds to cyclonic motions and negative to anticyclonic motions, which is the opposite convection compared to the one used by Cho and Lindborg (2001) and Lindborg and Cho (2001). As can be seen, cyclone-anticyclone symmetry is broken with different orientations in the two regions. The scale dependent skewness calculated from the tropospheric data is positive with a maximum of about unity at  $r \sim 500$  km, indicating that there is strong dominance of cyclonic motions. The skewness calculated from stratospheric data is negative, with a minimum of about minus two at  $r \sim 100$  km, indicating that there is strong dominance of anticyclonic motions.

Cyclone-anticyclone asymmetry is a fascinating and yet unsolved problem in fluid

mechanics. In homogeneous rotating turbulence there is a preference for cyclonic motions (Bartello et al. 1994; Morize and Moisy 2006; Staplehurst et al. 2008). The same seems to be true for homogeneous rotating stratified turbulence. Deusebio et al. (2014) carried out simulations of homogeneous rotating stratified turbulence to mimic the mesoscale motions and found that  $S(r) \approx 0.5$ . Unfortunately, there is a sign error of the corresponding stratospheric data that is plotted for comparison in figure 14 of Deusebio et al. (2014). In fact,  $S(r) \approx 0.5$  (positive) is in better agreement with the tropospheric data. For geophysical flows, it has been asserted that there is generally a preference for anticyclonic vortices (Graves et al. 2006), with the most famous example being the red spot of Jupiter. Simulations of the shallow water equations show strong dominance of anticyclones (Polvani et al. 1994; Stegner and Dritschel 2000). On the other hand, it has been observed that cyclones with characteristic radius of 500-1000 km are more common and stronger in the upper troposphere than anticyclones of the same size (Hakim 2000; Hakim and Canavan 2005), consistent with the results presented here. Hakim et al. (2002) developed a finite Rossby number surface quasigeostrophic model that was able to capture the dominance of cyclones near the tropopause. Roulet and Klein (2010) carried out high resolution simulations of the primitive equations with an active upper surface and found a strong preference for cyclonic motions close to the surface. They calculated  $S_\zeta$  both for the part of the field that is built up by coherent vortices and the background filamentary field, using the Okubo-Weiss criterion to distinguish vortices from filaments. They found strong symmetry breaking in the coherent field, with  $S_\zeta = 1.16$ , and even stronger symmetry breaking in the filamentary field, with  $S_\zeta = 1.96$ . In other words, symmetry breaking is not only caused by a dominance of coherent cyclones over coherent anticyclones. It is a property of the background filamentary field.

The degree to which cyclone-anticyclone symmetry is broken is non-monotonic in the strength of the rotation rate. When there is no rotation, there is, of course, no symmetry breaking. The same is true in the quasigeostrophic limit, since the quasigeostrophic equations are invariant under reflections (or parity invariant). The strongest degree of symmetry breaking is most often observed at rotation rates corresponding to Rossby numbers of the order of unity. The strong symmetry breaking in the mesoscale range in the upper troposphere and lower stratosphere fits very well into this picture, since the characteristic Rossby number of the mesoscale motions is of the order of unity (Li and Lindborg 2018). It is quite remarkable that the symmetry breaking has opposite orientations below and above the tropopause. Possibly, the tropopause acts as an active surface similar to the surface in the simulation by Roulet and Klein (2010), with dominance of cyclonic motions just below and anticyclonic motions just above – a hypothesis that would be interesting to test in numerical simulations.

### 3. Conclusions

The anisotropic Helmholtz decomposition problem for second order structure functions, including the reflectionally antisymmetric component, was formulated and completely solved. The solutions for the zero modes of the two reflectionally symmetric components were found to be identical to the corresponding solutions for the isotropic problem derived by Lindborg (2015), showing that these can be used even in anisotropic flows, provided that the structure functions are carefully averaged over all angles. The solution (2.14) and its spectral counterpart (2.26) for the reflectionally antisymmetric component may or may not become useful in future data analyses. The same can be said about the general anisotropic solutions (B 8-B 13) for the non-zero Fourier modes of the three components. In some cases, where there are plenty of two-dimensional data available from a particular site, they may become useful if the anisotropy of the flow is under investigation.

The most interesting new result that was derived is that there is a single component of the third order structure function that is associated with cyclone-anticyclone asymmetry of the vortical part of the horizontal velocity field and that this component can be used as a measure of the degree of symmetry breaking. In the light of the new analysis it is clear that the data analyses of Cho and Lindborg (2001) and Lindborg and Cho (2001) show that there is a strong preference for cyclonic motions in the upper troposphere and a strong preference for anticyclonic motions in the lower stratosphere in the range  $r \in [10, 1000]$  km. In the author's opinion, this observation falsifies the hypothesis developed by Callies et al. (2014), that the observed  $k^{-5/3}$ -spectra are generated by inertia-gravity waves. The observed symmetry breaking takes place only in the rotational component of the flow, which is as strong as the divergent component in the lower stratosphere and stronger in the upper troposphere (Li and Lindborg 2018). Moreover, the symmetry breaking is strong. There is no way a field of weakly non-linear inertia-gravity waves could display such effects. The observation clearly points to the presence of strong vortical motions governed by strongly nonlinear effects at Rossby number of the order of unity, as argued by Li and Lindborg (2018).

The observation that cyclone-anticyclone symmetry is broken with different orientations below and above the tropopause, is also somewhat problematic for the theory of vertically homogeneous stratified turbulence that was developed by Lindborg (2006) to explain the observed  $k^{-5/3}$  energy spectra. On the one hand, the theory captures essential features of the mesoscale motions: the partition between kinetic and available potential energy, the spectral shapes, the approximate equipartition between rotational and divergent kinetic energy and the downscale energy cascade. This is true also in the case when there is system rotation, provided that the Rossby number is of the order of unity (Deusebio et al. 2013). On the other hand, it is evident that no theory of vertically homogeneous turbulence can capture the opposite orientation of the cyclone-anticyclone asymmetry below and above the tropopause. This inevitable conclusion, which has been resisted by the author for many years, could have been drawn already on the basis of the results presented by Cho and Lindborg (2001).

**Acknowledgements** The author would like to thank J. Cho for sending him plots and data from the structure function analysis of Cho and Lindborg (2001).

**Declaration of interest** The author declares no conflict of interest.

## Appendix A. Derivation of 2.7-2.9 and 2.12-2.14

We let unprimed quantities be measured at  $\mathbf{x}$  and primed quantities at  $\mathbf{x}' = \mathbf{x} + \mathbf{r}$ . By statistical homogeneity we have

$$\langle \nabla_i^{\mathbf{x}} a(\mathbf{x}) \nabla_j^{\mathbf{x}'} b(\mathbf{x}') \rangle = -\nabla_i^{\mathbf{r}} \nabla_j^{\mathbf{r}} \langle ab' \rangle, \quad (\text{A } 1)$$

where  $a$  and  $b$  are any two scalar or vector functions. For simplicity, we write  $\nabla^{\mathbf{r}} = \nabla$ . By statistical homogeneity we also have

$$\nabla_i \langle ab \rangle = \nabla_i \langle a' b' \rangle = 0, \quad (\text{A } 2)$$



since  $\langle ab \rangle$  is a single-point quantity with no dependence on  $\mathbf{r}$  and  $\langle a'b' \rangle = \langle ab \rangle$ . By homogeneity, we find

$$\langle \zeta \zeta' \rangle = \nabla^4 \langle \psi \psi' \rangle, \quad (\text{A } 3)$$

$$\langle dd' \rangle = \nabla^4 \langle \phi \phi' \rangle, \quad (\text{A } 4)$$

$$\langle \zeta d' + \zeta' d \rangle = -\nabla^4 \langle \psi \phi' + \psi' \phi \rangle, \quad (\text{A } 5)$$

$$\begin{aligned} \nabla^2 \langle \delta \mathbf{u}_r \cdot \delta \mathbf{u}_r \rangle &= -2\nabla^2 \langle \mathbf{u}_r \cdot \mathbf{u}'_r \rangle = 2\nabla^2 (\mathbf{e}_z \times \nabla) \cdot (\mathbf{e}_z \times \nabla) \langle \psi \psi' \rangle \\ &= 2\nabla^4 \langle \psi \psi' \rangle, \end{aligned} \quad (\text{A } 6)$$

$$\nabla^2 \langle \delta \mathbf{u}_d \cdot \delta \mathbf{u}_d \rangle = -2\nabla^2 \langle \mathbf{u}_d \cdot \mathbf{u}'_d \rangle = 2\nabla^2 \nabla \cdot \nabla \langle \phi \phi' \rangle = 2\nabla^4 \langle \phi \phi' \rangle, \quad (\text{A } 7)$$

$$\begin{aligned} \nabla^2 (\mathbf{e}_z \cdot \langle \delta \mathbf{u}_d \times \delta \mathbf{u}_r \rangle) &= -\nabla^2 (\mathbf{e}_z \cdot \langle \mathbf{u}'_d \times \mathbf{u}_r \rangle + \mathbf{e}_z \cdot \langle \mathbf{u}_d \times \mathbf{u}'_r \rangle) \\ &= -\nabla^2 (\mathbf{e}_z \cdot (\nabla \times (\mathbf{e}_z \times \nabla)) \langle \psi \phi' + \psi' \phi \rangle) \\ &= -\nabla^4 \langle \psi \phi' + \psi' \phi \rangle. \end{aligned} \quad (\text{A } 8)$$

Combining (A 3) with (A 6), (A 4) with (A 7) and (A 5) with (A 8), we obtain (2.7), (2.8) and (2.9).

Equations (2.12-2.14) can be derived by expressing  $\mathbf{D}$  as a general tensor on a two-dimensional manifold using polar coordinates and then use the full machinery of Riemannian tensor analysis. However, since  $\mathbf{D}$  is defined on a plane, it is quite clear that it can also be expressed as a two-dimensional Cartesian tensor. We have found it more convenient to derive (2.12-2.14) using Cartesian tensor notation. Using such notation we have

$$\nabla^2 D_{dd} = 2\langle dd' \rangle = -\nabla_i \nabla_j \langle u_i u'_j + u_j u'_i \rangle = \nabla_i \nabla_j D_{ij}, \quad (\text{A } 9)$$

$$\nabla^2 D_{rr} = \nabla^2 (D_{ll} + D_{tt}) - \nabla^2 D_{dd}, \quad (\text{A } 10)$$

$$\nabla^2 D_{dr} = \langle \zeta d' + \zeta' d \rangle = -\epsilon_{3ki} \nabla_k \nabla_j \langle u_i u'_j + u'_i u_j \rangle = \epsilon_{3ki} \nabla_k \nabla_j D_{ij}, \quad (\text{A } 11)$$

where the indices should not be seen as referring to components with respect to a particular Cartesian coordinate system, but more as convenient tools to keep track on the contractions. To carry out the calculation, we use the following identities

$$\begin{aligned} \nabla_i &= \mathbf{e}_{li} \frac{\partial}{\partial r} + \mathbf{e}_{ti} \frac{1}{r} \frac{\partial}{\partial \theta}, \quad \frac{\partial \mathbf{e}_{li}}{\partial r} = \frac{\partial \mathbf{e}_{ti}}{\partial r} = 0, \\ \frac{\partial \mathbf{e}_{li}}{\partial \theta} &= \mathbf{e}_{ti}, \quad \frac{\partial \mathbf{e}_{ti}}{\partial \theta} = -\mathbf{e}_{li}, \quad \epsilon_{3ki} = \mathbf{e}_{lk} \mathbf{e}_{ti} - \mathbf{e}_{tk} \mathbf{e}_{li}, \\ \mathbf{e}_{li} \mathbf{e}_{li} &= \mathbf{e}_{ti} \mathbf{e}_{ti} = 1, \quad \mathbf{e}_{li} \mathbf{e}_{ti} = 0. \end{aligned} \quad (\text{A } 12)$$

A straightforward calculation gives

$$\begin{aligned}
\nabla^2 D_{dd} &= \nabla_i \left( \mathbf{e}_{lj} \frac{\partial}{\partial r} + \mathbf{e}_{tj} \frac{1}{r} \frac{\partial}{\partial \theta} \right) \left( \mathbf{e}_{li} \mathbf{e}_{lj} D_{ll} + \mathbf{e}_{ti} \mathbf{e}_{tj} D_{tt} + (\mathbf{e}_{li} \mathbf{e}_{tj} + \mathbf{e}_{ti} \mathbf{e}_{lj}) D_{lt} \right) \\
&= \left( \mathbf{e}_{li} \frac{\partial}{\partial r} + \mathbf{e}_{ti} \frac{1}{r} \frac{\partial}{\partial \theta} \right) \left( \mathbf{e}_{li} \left( \frac{\partial D_{ll}}{\partial r} + \frac{D_{ll}}{r} - \frac{D_{tt}}{r} + \frac{1}{r} \frac{\partial D_{lt}}{\partial \theta} \right) \right) \\
&\quad + \left( \mathbf{e}_{li} \frac{\partial}{\partial r} + \mathbf{e}_{ti} \frac{1}{r} \frac{\partial}{\partial \theta} \right) \left( \mathbf{e}_{ti} \left( \frac{1}{r} \frac{\partial D_{tt}}{\partial \theta} + \frac{\partial D_{lt}}{\partial r} + \frac{2D_{lt}}{r} \right) \right) \\
&= \left( \frac{\partial}{\partial r} + \frac{1}{r} \right) \left( \frac{\partial D_{ll}}{\partial r} + \frac{D_{ll}}{r} - \frac{D_{tt}}{r} + \frac{1}{r} \frac{\partial D_{lt}}{\partial \theta} \right) \\
&\quad + \frac{1}{r} \frac{\partial}{\partial \theta} \left( \frac{1}{r} \frac{\partial D_{tt}}{\partial \theta} + \frac{\partial D_{lt}}{\partial r} + \frac{2D_{lt}}{r} \right) \\
&= \nabla^2 D_{tt} + \frac{\partial^2 (D_{ll} - D_{tt})}{\partial r^2} + \frac{2}{r} \frac{\partial (D_{ll} - D_{tt})}{\partial r} + \frac{2}{r} \frac{\partial^2 D_{lt}}{\partial r \partial \theta} + \frac{2}{r^2} \frac{\partial D_{lt}}{\partial \theta} \\
&= \nabla^2 D_{tt} + \frac{1}{r^2} \frac{\partial}{\partial r} \left( r^2 \frac{\partial (D_{ll} - D_{tt})}{\partial r} \right) + \frac{2}{r^2} \frac{\partial}{\partial r} \left( r \frac{\partial D_{lt}}{\partial \theta} \right) \\
\nabla^2 D_{rr} &= \nabla^2 D_{ll} - \frac{1}{r^2} \frac{\partial}{\partial r} \left( r^2 \frac{\partial (D_{ll} - D_{tt})}{\partial r} \right) - \frac{2}{r^2} \frac{\partial}{\partial r} \left( r \frac{\partial D_{lt}}{\partial \theta} \right)
\end{aligned} \tag{A13}$$

$$\begin{aligned}
\nabla^2 D_{dr} &= (\mathbf{e}_{lk} \mathbf{e}_{ti} - \mathbf{e}_{tk} \mathbf{e}_{li}) \left( \mathbf{e}_{lk} \frac{\partial}{\partial r} + \mathbf{e}_{tk} \frac{1}{r} \frac{\partial}{\partial \theta} \right) \nabla_j D_{ij} \\
&= \left( \mathbf{e}_{ti} \frac{\partial}{\partial r} - \mathbf{e}_{li} \frac{1}{r} \frac{\partial}{\partial \theta} \right) \left( \mathbf{e}_{li} \left( \frac{\partial D_{ll}}{\partial r} + \frac{D_{ll}}{r} - \frac{D_{tt}}{r} + \frac{1}{r} \frac{\partial D_{lt}}{\partial \theta} \right) \right) \\
&\quad + \left( \mathbf{e}_{ti} \frac{\partial}{\partial r} - \mathbf{e}_{li} \frac{1}{r} \frac{\partial}{\partial \theta} \right) \left( \mathbf{e}_{ti} \left( \frac{1}{r} \frac{\partial D_{tt}}{\partial \theta} + \frac{\partial D_{lt}}{\partial r} + \frac{2D_{lt}}{r} \right) \right) \\
&= -\frac{1}{r} \frac{\partial}{\partial \theta} \left( \frac{\partial D_{ll}}{\partial r} + \frac{D_{ll}}{r} - \frac{D_{tt}}{r} + \frac{1}{r} \frac{\partial D_{lt}}{\partial \theta} \right) \\
&\quad + \left( \frac{\partial}{\partial r} + \frac{1}{r} \right) \left( \frac{1}{r} \frac{\partial D_{tt}}{\partial \theta} + \frac{\partial D_{lt}}{\partial r} + \frac{2D_{lt}}{r} \right) \\
&= \frac{1}{r^2} \frac{\partial}{\partial r} \left( r^2 \frac{\partial D_{lt}}{\partial r} \right) + \frac{1}{r} \frac{\partial D_{lt}}{\partial r} - \frac{1}{r^2} \frac{\partial^2 D_{lt}}{\partial \theta^2} + \frac{1}{r^2} \frac{\partial^2}{\partial r \partial \theta} (r(D_{tt} - D_{ll}))
\end{aligned} \tag{A14}$$

## Appendix B. Solutions for the non-zero modes

The solutions for each of the Fourier modes of the structure functions can be found by expressing the Laplacian of  $f(r, \theta)$  as

$$\begin{aligned}
\nabla^2 f &= \frac{\partial^2 f}{\partial r^2} + \frac{1}{r} \frac{\partial f}{\partial r} + \frac{1}{r^2} \frac{\partial^2 f}{\partial \theta^2} \\
&= \sum_{n=2k} r^{n-1} \left[ \frac{d}{dr} \left( r^{1-2n} \frac{d}{dr} (r^n f^{cn}) \right) \cos(n\theta) + \frac{d}{dr} \left( r^{1-2n} \frac{d}{dr} (r^n f^{sn}) \right) \sin(n\theta) \right].
\end{aligned} \tag{B1}$$

Thus, for a mode of order  $p$  we have an equation of the form

$$r^{p-1} \frac{d}{dr} \left( r^{1-2p} \frac{d}{dr} (r^p f^p) \right) = m(r), \quad (\text{B } 2)$$

which can be inverted as

$$f^p(r) = -r^{-p} \int_0^r \eta^{2p-1} \int_\eta^\infty \tau^{-p+1} m(\tau) d\tau d\eta. \quad (\text{B } 3)$$

We derive four inversion formulas for  $p \neq 0$ , which will be used to construct the solutions. First, we set  $m(\tau) = \tau^{-2} d_\tau (\tau^2 d_\tau g(\tau))$ ,

$$\begin{aligned} & -r^{-p} \int_0^r \eta^{2p-1} \int_\eta^\infty \tau^{-p-1} \frac{d}{d\tau} \left( \tau^2 \frac{dg}{d\tau} \right) d\tau d\eta \\ &= -\frac{1}{2p} r^p \int_r^\infty \tau^{-p-1} \frac{d}{d\tau} \left( \tau^2 \frac{dg}{d\tau} \right) d\tau - \frac{1}{2p} r^{-p} \int_0^r \tau^{p-1} \frac{d}{d\tau} \left( \tau^2 \frac{dg}{d\tau} \right) d\tau \\ &= -\frac{1}{2p} r^p \left[ \tau^{-p+1} \frac{dg}{d\tau} \right]_r^\infty - \frac{1}{2p} r^{-p} \left[ \tau^{p+1} \frac{dg}{d\tau} \right]_0^r \\ & - \frac{(p+1)}{2p} r^p \int_r^\infty \tau^{-p} \frac{dg}{d\tau} d\tau + \frac{p-1}{2p} r^{-p} \int_0^r \tau^p \frac{dg}{d\tau} d\tau \quad (\text{B } 4) \\ &= -\frac{(p+1)}{2p} r^p [\tau^{-p} g(\tau)]_r^\infty + \frac{(p-1)}{2p} r^{-p} [\tau^p g(\tau)]_0^r \\ & - \frac{1}{2} (p+1) r^p \int_r^\infty \tau^{-p-1} g(\tau) d\tau - \frac{1}{2} (p-1) r^{-p} \int_0^r \tau^{p-1} g(\tau) d\tau \\ &= g(r) - \frac{1}{2} r^p \int_r^\infty \tau^{-p-1} (p+1) g(\tau) d\tau - \frac{1}{2} r^{-p} \int_0^r \tau^{p-1} (p-1) g(\tau) d\tau. \end{aligned}$$

Then we set  $m(\tau) = \tau^{-1} d_\tau h(\tau)$ ,

$$\begin{aligned} & -r^{-p} \int_0^r \eta^{2p-1} \int_\eta^\infty \tau^{-p} \frac{dh}{d\tau} d\tau d\eta \\ &= -\frac{1}{2p} r^p \int_r^\infty \tau^{-p} \frac{dh}{d\tau} d\tau - \frac{1}{2p} r^{-p} \int_0^r \tau^p \frac{dh}{d\tau} d\tau \\ &= -\frac{1}{2p} r^p [\tau^{-p} h(\tau)]_r^\infty - \frac{1}{2p} r^{-p} [\tau^p h(\tau)]_0^r \quad (\text{B } 5) \\ & - \frac{1}{2} r^p \int_r^\infty \tau^{-p-1} h(\tau) d\tau + \frac{1}{2} r^{-p} \int_0^r \tau^{p-1} h(\tau) d\tau \\ &= -\frac{1}{2} r^p \int_r^\infty \tau^{-p-1} h(\tau) d\tau + \frac{1}{2} r^{-p} \int_0^r \tau^{p-1} h(\tau) d\tau. \end{aligned}$$

Then we set  $m(\tau) = \tau^{-2}d_\tau(\tau q(\tau))$ ,

$$\begin{aligned}
& -r^{-p} \int_0^r \eta^{2p-1} \int_\eta^\infty \tau^{-p-1} \frac{d}{d\tau} (\tau q(\tau)) d\tau d\eta \\
&= -\frac{1}{2p} r^p \int_r^\infty \tau^{-p-1} \frac{d}{d\tau} (\tau q(\tau)) d\tau - \frac{1}{2p} r^{-p} \int_0^r \tau^{p-1} \frac{d}{d\tau} (\tau q(\tau)) d\tau \\
&= -\frac{1}{2p} r^p [\tau^{-p} q(\tau)]_r^\infty - \frac{1}{2p} r^{-p} [\tau^p q(\tau)]_0^r \\
& -\frac{p+1}{2p} r^p \int_r^\infty \tau^{-p-1} q(\tau) d\tau + \frac{p-1}{2p} r^{-p} \int_0^r \tau^{p-1} q(\tau) d\tau \\
&= -\frac{1}{2p} r^p \int_r^\infty \tau^{-p-1} (p+1) q(\tau) d\tau + \frac{1}{2p} r^{-p} \int_0^r \tau^{p-1} (p-1) q(\tau) d\tau.
\end{aligned} \tag{B 6}$$

Finally, we set  $m(\tau) = \tau^{-2}s(\tau)$ ,

$$\begin{aligned}
& -r^{-p} \int_0^r \eta^{2p-1} \int_\eta^\infty \tau^{-p-1} s(\tau) d\tau d\eta \\
&= -\frac{1}{2p} r^p \int_r^\infty \tau^{-p-1} s(\tau) d\tau - \frac{1}{2p} r^{-p} \int_0^r \tau^{p-1} s(\tau) d\tau.
\end{aligned} \tag{B 7}$$

The solution for  $D_{rr}^{cP}$  ( $p \neq 0$ ) is constructed by putting  $g(\tau) = D_{tt}^{cP}(\tau) - D_{ll}^{cP}(\tau)$  and  $q(\tau) = -2pD_{tt}^{sP}(\tau)$  and the solution for  $D_{rr}^{sP}$  is constructed in a corresponding way,

$$\begin{aligned}
D_{rr}^{cP}(r) &= D_{tt}^{cP}(r) \\
& -\frac{1}{2}(p+1)r^p \int_r^\infty \tau^{-p-1} \left( D_{tt}^{cP}(\tau) - D_{ll}^{cP}(\tau) - 2D_{tt}^{sP}(\tau) \right) d\tau \\
& -\frac{1}{2}(p-1)r^{-p} \int_0^r \tau^{p-1} \left( D_{tt}^{cP}(\tau) - D_{ll}^{cP}(\tau) + 2D_{tt}^{sP}(\tau) \right) d\tau,
\end{aligned} \tag{B 8}$$

$$\begin{aligned}
D_{rr}^{sP}(r) &= D_{tt}^{sP}(r) \\
& -\frac{1}{2}(p+1)r^p \int_r^\infty \tau^{-p-1} \left( D_{tt}^{sP}(\tau) - D_{ll}^{sP}(\tau) + 2D_{tt}^{cP}(\tau) \right) d\tau \\
& -\frac{1}{2}(p-1)r^{-p} \int_0^r \tau^{p-1} \left( D_{tt}^{sP}(\tau) - D_{ll}^{sP}(\tau) - 2D_{tt}^{cP}(\tau) \right) d\tau.
\end{aligned} \tag{B 9}$$

The solutions for  $D_{dd}^{cP}$  and  $D_{dd}^{sP}$  are then given by

$$D_{dd}^{cP}(r) = D_{ll}^{cP}(r) + D_{tt}^{cP}(r) - D_{rr}^{cP}(r), \tag{B 10}$$

$$D_{dd}^{sP}(r) = D_{ll}^{sP}(r) + D_{tt}^{sP}(r) - D_{rr}^{sP}(r). \tag{B 11}$$

The solution for  $D_{dr}^{cP}$  ( $p \neq 0$ ) is constructed by putting  $g(\tau) = h(\tau) = D_{tt}^{cP}(\tau)$ ,  $s(\tau) = p^2 D_{tt}^{cP}(\tau)$ , and  $q(\tau) = p(D_{tt}^{sP}(\tau) - D_{ll}^{sP}(\tau))$  and the solution for  $D_{dr}^{sP}$  is constructed in the

corresponding way,

$$\begin{aligned}
D_{dr}^{cP}(r) &= D_{lt}^{cP}(r) \\
&\quad - \frac{1}{2}(p+1)r^p \int_r^\infty \tau^{-p-1} \left( D_{tt}^{sP}(\tau) - D_{ll}^{sP}(\tau) + 2D_{lt}^{cP}(\tau) \right) d\tau \\
&\quad + \frac{1}{2}(p-1)r^{-p} \int_0^r \tau^{p-1} \left( D_{tt}^{sP}(\tau) - D_{ll}^{sP}(\tau) - 2D_{lt}^{cP}(\tau) \right) d\tau, \tag{B 12}
\end{aligned}$$

$$\begin{aligned}
D_{dr}^{sP}(r) &= D_{lt}^{sP}(r) \\
&\quad + \frac{1}{2}(p+1)r^p \int_r^\infty \tau^{-p-1} \left( D_{tt}^{cP}(\tau) - D_{ll}^{cP}(\tau) - 2D_{lt}^{sP}(\tau) \right) d\tau \\
&\quad - \frac{1}{2}(p-1)r^{-p} \int_0^r \tau^{p-1} \left( D_{tt}^{cP}(\tau) - D_{ll}^{cP}(\tau) + 2D_{lt}^{sP}(\tau) \right) d\tau. \tag{B 13}
\end{aligned}$$

We note that the two integrals in (B 12) are identical to the integrals in (B 9), apart from the sign of the second, and that the two integrals in (B 13) are identical to the integrals in (B 8), apart from the sign of the first.

### Appendix C. The solutions derived by Wang and Bühler (2021)

In this Appendix, we confirm that the solutions derived by Wang and Bühler (2021) are correct, given the assumption under which they were derived. Having guessed at solutions for the Fourier modes and verified these by the aid of computer algebra, Wang and Bühler (2021) were able to sum all the modes and write the final solutions in the compact form

$$D_{rr}(r, \theta) = D_{tt}(r, \theta) + \int_0^r \tau^{-1} \left( D_{tt}(\tau, \theta) - D_{ll}(\tau, \theta) - \frac{\partial D_{lt}}{\partial \theta}(\tau, \theta) \right) d\tau, \tag{C 1}$$

$$D_{dd}(r, \theta) = D_{ll}(r, \theta) - \int_0^r \tau^{-1} \left( D_{tt}(\tau, \theta) - D_{ll}(\tau, \theta) - \frac{\partial D_{lt}}{\partial \theta}(\tau, \theta) \right) d\tau. \tag{C 2}$$

Expressions (C 1) and (C 2) are correct solutions if (C 1) satisfies (2.12) and (C 2) satisfies (2.13) and if they have the correct  $r^2$ -dependence in the limit  $r \rightarrow 0$  and are bounded in the limit  $r \rightarrow \infty$ . The condition for the limit  $r \rightarrow 0$  is trivially fulfilled and the condition that the expressions are bounded in the limit  $r \rightarrow \infty$  is also fulfilled, which can be verified by substituting (2.22-2.23) into the integrals. We will now prove that (C 1) satisfies (2.12) if and only if the two-point covariance of divergence and vorticity is not a function of  $\theta$ , which can be formulated as

$$\partial_\theta \nabla^2 D_{dr} = 0. \tag{C 3}$$

Taking the Laplace of (C1) we obtain

$$\begin{aligned}
\nabla^2 D_{rr} &= \nabla^2 D_{tt} + \frac{1}{r} \frac{\partial}{\partial r} \left( D_{tt} - D_{ll} - \frac{\partial D_{lt}}{\partial \theta} \right) \\
&+ \frac{1}{r^2} \int_0^r \tau^{-1} \frac{\partial^2}{\partial \theta^2} \left( D_{tt} - D_{ll} - \frac{\partial D_{lt}}{\partial \theta} \right) d\tau \\
&= \nabla^2 D_{ll} + \frac{1}{r^2} \frac{\partial}{\partial r} \left( r^2 \frac{\partial (D_{tt} - D_{ll})}{\partial r} \right) + \frac{1}{r^2} \frac{\partial^2}{\partial \theta^2} (D_{tt} - D_{ll}) - \frac{1}{r} \frac{\partial^2 D_{lt}}{\partial r \partial \theta} \\
&+ \frac{1}{r^2} \int_0^r \tau^{-1} \frac{\partial^2}{\partial \theta^2} \left( D_{tt} - D_{ll} - \frac{\partial D_{lt}}{\partial \theta} \right) d\tau \\
&= \nabla^2 D_{ll} + \frac{1}{r^2} \frac{\partial}{\partial r} \left( r^2 \frac{\partial (D_{tt} - D_{ll})}{\partial r} \right) - \frac{1}{r} \frac{\partial^2 D_{lt}}{\partial r \partial \theta} \\
&+ \frac{1}{r^2} \int_0^r \tau^{-1} \frac{\partial}{\partial \tau} \left( \tau \frac{\partial^2}{\partial \theta^2} (D_{tt} - D_{ll}) \right) - \tau^{-1} \frac{\partial^3 D_{lt}}{\partial \theta^3} d\tau.
\end{aligned} \tag{C4}$$

Applying  $\partial_\theta$  to (2.14) under the condition (C3), yields

$$\tau^{-1} \frac{\partial}{\partial \tau} \left( \tau \frac{\partial^2}{\partial \theta^2} (D_{tt} - D_{ll}) \right) = \tau^{-1} \frac{\partial^3 D_{lt}}{\partial \theta^3} - \frac{1}{\tau} \frac{\partial}{\partial \tau} \left( \tau^2 \frac{\partial^2 D_{lt}}{\partial \tau \partial \theta} \right) - \frac{\partial^2 D_{lt}}{\partial \tau \partial \theta}. \tag{C5}$$

Substituting (C5) into the integral in (C4) and integrating by parts, we finally obtain

$$\nabla^2 D_{rr} = \nabla^2 D_{ll} + \frac{1}{r^2} \frac{\partial}{\partial r} \left( r^2 \frac{\partial (D_{tt} - D_{ll})}{\partial r} \right) - \frac{2}{r^2} \frac{\partial}{\partial r} \left( r \frac{\partial D_{lt}}{\partial \theta} \right), \tag{C6}$$

which is identical to (2.12). That (C2) satisfies (2.13) now follows directly from (2.11). It is quite remarkable that (C1) and (C2) are solutions to (2.12) and (2.13) under the condition (C3). It is clear that (C3) is a necessary and sufficient condition. We have found no other method to prove this than by direct verification, which is similar to the method used by Wang and Bühler (2021), although they used a set of equations that appears to be completely different than we have used.

## Appendix D. Third order structure function calculations

We first determine the components of  $\mathbf{P}$  and  $\mathbf{Q}$ , by carrying out the calculations using Cartesian tensor notation.

$$\begin{aligned}
P_{ij} &= \nabla_k D_{kij}^{(3)} = \left( e_{lk} \frac{\partial}{\partial r} + e_{tk} \frac{1}{r} \frac{\partial}{\partial \theta} \right) D_{kij}^{(3)} \\
&= \left( e_{lk} \frac{\partial}{\partial r} + e_{tk} \frac{1}{r} \frac{\partial}{\partial \theta} \right) (e_{lk} e_{li} e_{lj} D_{lll} + (e_{lk} e_{ti} e_{tj} + e_{tk} e_{li} e_{tj} + e_{tk} e_{ti} e_{lj}) D_{ltt}) \\
&+ \left( e_{lk} \frac{\partial}{\partial r} + e_{tk} \frac{1}{r} \frac{\partial}{\partial \theta} \right) (e_{tk} e_{ti} e_{tj} D_{ttt} + (e_{tk} e_{li} e_{lj} + e_{lk} e_{ti} e_{lj} + e_{lk} e_{li} e_{tj}) D_{tll}) \\
&= e_{li} e_{lj} \left( \frac{dD_{lll}}{dr} + \frac{D_{lll}}{r} - 2 \frac{D_{ltt}}{r} \right) + e_{ti} e_{tj} \left( \frac{dD_{ltt}}{dr} + 3 \frac{D_{ltt}}{r} \right) \\
&+ (e_{li} e_{tj} + e_{ti} e_{lj}) \left( \frac{dD_{tll}}{dr} + 2 \frac{D_{tll}}{r} - \frac{D_{ttt}}{r} \right)
\end{aligned} \tag{D1}$$

$$\begin{aligned}
Q_{ij} &= \epsilon_{3km} \nabla_k D_{mij}^{(3)} = (\mathbf{e}_{lk} \mathbf{e}_{tm} - \mathbf{e}_{tk} \mathbf{e}_{lm}) \left( \mathbf{e}_{lk} \frac{\partial}{\partial r} + \mathbf{e}_{tk} \frac{1}{r} \frac{\partial}{\partial \theta} \right) D_{mij}^{(3)} \\
&= \left( \mathbf{e}_{tm} \frac{\partial}{\partial r} - \mathbf{e}_{lm} \frac{1}{r} \frac{\partial}{\partial \theta} \right) (\mathbf{e}_{lm} \mathbf{e}_{li} \mathbf{e}_{lj} D_{lll} + (\mathbf{e}_{lm} \mathbf{e}_{ti} \mathbf{e}_{tj} + \mathbf{e}_{tm} \mathbf{e}_{li} \mathbf{e}_{tj} + \mathbf{e}_{tm} \mathbf{e}_{ti} \mathbf{e}_{lj}) D_{ltt}) \\
&+ \left( \mathbf{e}_{tm} \frac{\partial}{\partial r} - \mathbf{e}_{lm} \frac{1}{r} \frac{\partial}{\partial \theta} \right) (\mathbf{e}_{tm} \mathbf{e}_{ti} \mathbf{e}_{tj} D_{ttt} + (\mathbf{e}_{tm} \mathbf{e}_{li} \mathbf{e}_{lj} + \mathbf{e}_{lm} \mathbf{e}_{ti} \mathbf{e}_{lj} + \mathbf{e}_{lm} \mathbf{e}_{li} \mathbf{e}_{tj}) D_{tll}) \quad (\text{D } 2) \\
&= \mathbf{e}_{li} \mathbf{e}_{lj} \left( \frac{dD_{tll}}{dr} + 3 \frac{D_{tll}}{r} \right) + \mathbf{e}_{ti} \mathbf{e}_{tj} \left( \frac{dD_{ttt}}{dr} + \frac{D_{ttt}}{r} - 2 \frac{D_{tll}}{r} \right) \\
&+ (\mathbf{e}_{li} \mathbf{e}_{tj} + \mathbf{e}_{ti} \mathbf{e}_{lj}) \left( \frac{dD_{ltt}}{dr} + 2 \frac{D_{ltt}}{r} - \frac{D_{lll}}{r} \right)
\end{aligned}$$

Next, we show that  $Q_{dd} = P_{dr}$  and  $Q_{dr} = P_{rr}$ ,

$$Q_{dd} = \nabla_i \nabla_j \epsilon_{3km} \nabla_k D_{mij}^{(3)} \quad (\text{D } 3)$$

$$P_{dr} = \epsilon_{3km} \nabla_k \nabla_i \nabla_j D_{jmi}^{(3)} = \nabla_i \nabla_j \epsilon_{3km} \nabla_k D_{mij}^{(3)} = Q_{dd}, \quad (\text{D } 4)$$

$$Q_{dr} = \epsilon_{3kn} \nabla_k \nabla_i \epsilon_{3sm} \nabla_s D_{min}^{(3)} = \epsilon_{3kn} \epsilon_{3sm} \nabla_k \nabla_s \nabla_i D_{nmi}^{(3)}, \quad (\text{D } 5)$$

$$P_{rr} = \epsilon_{3kn} \epsilon_{3sm} \nabla_k \nabla_s \nabla_i D_{nmi}^{(3)} = Q_{dr}. \quad (\text{D } 6)$$

We proceed by proving (2.31) and (2.32). For an exclusively rotational field we have  $P_{dd} = 0$ . Using equation (2.13) for  $P_{dd}$  instead of  $D_{dd}$  we obtain

$$\begin{aligned}
\nabla^2 P_{dd} &= -\frac{1}{r} \frac{dP_{ll}}{dr} + \frac{1}{r^2} \frac{d}{dr} \left( r^2 \frac{dP_{tt}}{dr} \right) \\
&= -\frac{3}{r} \frac{d^2 D_{ltt}}{dr^2} - \frac{3}{r^2} \frac{dD_{ltt}}{dr} + \frac{3D_{ltt}}{r^3} + \frac{d^3 D_{lll}}{dr^3} + \frac{3}{r} \frac{d^2 D_{lll}}{dr^2} \\
&= -\frac{3}{r} \frac{d}{dr} \left( \frac{1}{r} \frac{d}{dr} (r D_{ltt}) \right) + \frac{1}{r^3} \frac{d}{dr} \left( r^3 \frac{d^2 D_{ttt}}{dr^2} \right). \quad (\text{D } 7)
\end{aligned}$$

Putting the left hand side of (D 7) to zero, multiplying by  $r$ , and integrating twice, we find

$$D_{ltt} = \frac{r}{3} \frac{dD_{lll}}{dr}, \quad (\text{D } 8)$$

which proves (2.31). For an exclusively rotational field we also have  $P_{dr} = 0$ . Using equation (2.14) for  $P_{dr}$  instead of  $D_{dr}$  we obtain

$$\nabla^2 P_{dr} = \frac{1}{r^3} \frac{d}{dr} \left( r^3 \frac{dP_{lt}}{dr} \right) = \frac{1}{r^3} \frac{d}{dr} \left( r^3 \frac{d}{dr} \left( \frac{dD_{tll}}{dr} + 2 \frac{D_{tll}}{r} - \frac{D_{ttt}}{r} \right) \right). \quad (\text{D } 9)$$

Putting the left hand side of (D 9) to zero, multiplying by  $r^3$ , integrating twice and requiring bounded solutions, we obtain

$$D_{ttt} = \frac{1}{r} \frac{d}{dr} \left( r^2 D_{tll} \right), \quad (\text{D } 10)$$

which proves (2.32). Finally, we prove (2.34) and (2.35). For a divergent field we have  $P_{rr} = Q_{dr} = 0$ . Using equation (2.14) for  $Q_{dr}$  instead of  $D_{dr}$  we obtain

$$\nabla^2 Q_{dr} = \frac{1}{r^3} \frac{d}{dr} \left( r^3 \frac{dQ_{lt}}{dr} \right) = \frac{1}{r^3} \frac{d}{dr} \left( r^3 \frac{d}{dr} \left( \frac{dD_{ltt}}{dr} + 2 \frac{D_{ltt}}{r} - \frac{D_{lll}}{r} \right) \right). \quad (\text{D } 11)$$

The expression (D 11) is identically zero if and only if

$$D_{lll} = \frac{1}{r} \frac{d}{dr} \left( r^2 D_{lll} \right), \quad (\text{D } 12)$$

which proves (2.34). For a divergent field we have  $P_{dr} = 0$ , implying (D 10). In addition, we have  $Q_{rr} = 0$ . Using equation (2.12) for  $Q_{rr}$  instead of  $D_{rr}$  we obtain

$$\begin{aligned} \nabla^2 Q_{rr} &= -\frac{1}{r} \frac{dQ_{ll}}{dr} + \frac{1}{r^2} \frac{d}{dr} \left( r^2 \frac{dQ_{ll}}{dr} \right) \\ &= -\frac{3}{r} \frac{d^2 D_{lll}}{dr^2} - \frac{3}{r^2} \frac{dD_{lll}}{dr} + \frac{3D_{lll}}{r^3} + \frac{d^3 D_{lll}}{dr^3} + \frac{3}{r} \frac{d^2 D_{lll}}{dr^2}. \end{aligned} \quad (\text{D } 13)$$

The expression (D 13) is identically zero if and only if

$$D_{lll} = \frac{r}{3} \frac{dD_{lll}}{dr}. \quad (\text{D } 14)$$

For a divergent field both (D 10) and (D 14) must hold, implying that

$$\frac{d^2 D_{lll}}{dr^2} + \frac{3}{r} \frac{dD_{lll}}{dr} - \frac{3D_{lll}}{r^2} = 0. \quad (\text{D } 15)$$

The only bounded solution to (D 15) satisfying  $D_{lll}(0) = 0$  is  $D_{lll} = 0$ , also implying that  $D_{lll} = 0$ . This proves (2.35).

#### REFERENCES

- BARTELLO, P., MÉTAIS, O. & LESIEUR, M. 1994 Coherent structures in rotating three-dimensional turbulence *J. Fluid Mech.*, **273**, 1–29
- BÜHLER, O., CALLIES, J. & FERRARI, R. 2014 Wave–vortex decomposition of one-dimensional ship-track data *J. Fluid Mech.*, **756**, 1007–1026
- BÜHLER, O., KUANG, M. & TABAK, E.G. 2017 Anisotropic Helmholtz and wave–vortex decomposition of one-dimensional spectra *J. Fluid Mech.*, **815**, 361–387
- CALLIES, J., FERRARI, R. & BÜHLER, O. 2014 Transition from geostrophic turbulence to inertia–gravity waves in the atmospheric energy spectrum *Proc. Natl. Acad. Sci. USA*, **111**, 17 033–17 038
- CALLIES, J., BÜHLER, O. & FERRARI, R. 2016 The dynamics of mesoscale winds in the upper troposphere and lower stratosphere *J. Atmos. Sci.*, **73**, 4853–4872
- CALLIES, J., BARKAN, R. & GARABATO, A.N. 2020 Time scales of submesoscale flow inferred from a mooring array *J. Phys. Oceanogr.*, **50**, 1065–1086
- CHO, Y. N. & NEWELL, R. E. 1999 Horizontal wavenumber spectra of winds, temperature, and trace gases during the Pacific Exploratory Missions: 2. Gravity waves, quasi-two-dimensional turbulence, and vortical modes *J. Geophys. Res.* **104** (D13), 16297–16308
- CHO, J.Y.N. & LINDBORG, E. 2001 Horizontal velocity structure functions in the upper troposphere and lower stratosphere: 1. Observations *J. Geophys. Res. Atmos.*, **106**, 10233–10241
- DEUSEBIO, E., VALLGREN, A. & LINDBORG, E. 2013 The route to dissipation in strongly stratified and rotating flows *J. Fluid Mech.*, **720**, 66–103
- DEUSEBIO, E., AUGIER, P. & LINDBORG, E. 2014 Third-order structure functions in rotation and stratified turbulence: a comparison between numerical, analytical and observational results *J. Fluid Mech.*, **755**, 294–313
- ECKERMANN, S.D. 1990 Effects of Nonstationarity on Spectral Analysis of Mesoscale Motions in the Atmosphere *J. Geophys. Res.*, **95**, (D10) 16685–16703
- GRAVES, L.P., McWILLIAMS, J.C. & MONTGOMERY, M.T. 2006 Vortex evolution due to straining: a mechanism for dominance of strong, interior anticyclones *Geophys. Astrophys. Fluid Dyn.*, **100**, 151–183
- HAKIM, G.J. 2000 Climatology of coherent structures on the extratropical tropopause *Mon. Wea. Rev.*, **128**, 385–406
- HAKIM, G.J., SNYDER, C. & MURAKI, D.J. 2002 A New Surface Model for Cyclone–Anticyclone Asymmetry *J. Atmos. Sci.*, **59**, 2405–2420

- HAKIM, G.J. & CANAVAN, A.K. 2005 Observed Cyclone-Anticyclone Tropopause Asymmetries *J. Atmos. Sci.*, **62**, 231-240
- LI, Q. & LINDBORG, E. 2018 Weakly or strongly nonlinear dynamics close to the tropopause? *J. Atmos. Sci.*, **75**, 1215-1229
- LINDBORG, E. 1999 Can the atmospheric energy spectrum be explained by two-dimensional turbulence? *J. Fluid Mech.*, **388**, 259-288
- LINDBORG, E. & CHO, J.Y.N. 2001 Horizontal velocity structure functions in the upper troposphere and lower stratosphere: 1. Theoretical considerations *J. Geophys. Res. Atmos.*, **106**, 10223-10232
- LINDBORG, E. 2006 The energy cascade in a strongly stratified fluid *J. Fluid Mech.*, **550**, 207-242
- LINDBORG, E. 2007 Horizontal wavenumber spectra of vertical vorticity and horizontal divergence in the upper troposphere and lower stratosphere. *J. Atmos. Sci.*, **64**, 1017-1025
- LINDBORG, E. 2015 A Helmholtz decomposition of structure functions and spectra calculated from aircraft data *J. Fluid Mech.*, **762**. R4
- MORIZE, C. & MOISY, F. 2006 On the energy decay of rotating turbulence in confined geometry *Phys. Fluids* **18**, 065107
- NASTROM, G. D. & GAGE, K. S. 1985 A climatology of atmospheric wavenumber spectra of wind and temperature observed by commercial aircraft *J. Atmos. Sci.*, **42**, 950-960
- PEARSON, J., FOX-KEMPER, B., BARKAN, R., CHOI, J., BRACCO, A. & McWILLIAMS, J.C. 2019 Impacts of convergence on structure functions from surface drifters in the Gulf of Mexico *J. Phys. Oceanogr.*, **49**, 675-69
- POBLET, F. L., VIERINEN, J., AVSARKISOV, V., CONTE, J. F., CHARUVIL ASOKAN, H., JACOBI, C. & CHAU, J. L. 2023 Horizontal correlation functions of wind fluctuations in the mesosphere and lower thermosphere *J. Geophys. Res. Atmos.*, **28**, e2022JD03809
- POLVANI, L.M., McWILLIAMS, J.C., SPALL, M.A. & FORD, R. 1994 The coherent structures of shallow-water turbulence: Deformation-radius effects, cyclone/anticyclone asymmetry and gravity-wave generation *Chaos*, **4**, 177-186
- ROULLET, G. & KLEIN, P. 2010 Cyclone-Anticyclone Asymmetry in Geophysical Turbulence *Phys. Rev. Lett.*, **104**, 218501
- STAPLEHURST, P. J., DAVIDSON, P. A. & DALZIEL, S. B. 2008 Structure formation in homogeneous freely decaying rotating turbulence *J. Fluid Mech.*, **598**, 81-105.
- STEGNER, A. & DRITSCHEL, D.G. 2000 A numerical Investigation of the Stability of Isolated Shallow Water Vortices *J. Phys. Ocean.*, **30**, 2562-2573
- VLADOIU, A., LIEN, R.-C. & KUNZE, E. 2024 Energy partition between Submesoscale Internal Waves and Quasigeostrophic Vortical Motion in the Pycnocline *J. Phys. Oceanogr.*, **54**, 1285-1306
- WANG, H. & BÜHLER, O. 2021 Anisotropic Statistics of Lagrangian Structure Functions and Helmholtz Decomposition *J. Phys. Oceanogr.*, **51**, 1375-1393
- ZHURBAS, V., VÄLI, G., & KUZMIN, N. 2019 Rotation of floating particles in submesoscale cyclonic and anticyclonic eddies: a model study for the southeastern Baltic Sea *Ocean Sci.*, **15**, 1691-1705